Materials Today Bio 15 (2022) 100280

Contents lists available at ScienceDirect

Materials Today Bio

journal homepage: www.journals.elsevier.com/materials-today-bio

Fusing spheroids to aligned μ-tissues in a heart-on-chip featuring oxygen sensing and electrical pacing capabilities

Oliver Schneider [a], Alessia Moruzzi [b,d], Stefanie Fuchs [c], Alina Grobel [a], Henrike S. Schulze [a], Torsten Mayr [c], Peter Loskill [b,d,e,*]

[a] Fraunhofer Institute for Interfacial Engineering and Biotechnology IGB, Stuttgart, Germany
[b] NMI Natural and Medical Sciences Institute at the University of Tübingen, Reutlingen, Germany
[c] Institute for Analytical Chemistry and Food Chemistry, Graz University of Technology, Graz, Austria
[d] Department for Microphysiological Systems, Institute of Biomedical Engineering, Eberhard Karls University Tübingen, Tübingen, Germany
[e] 3R-Center for In vitro Models and Alternatives to Animal Testing, Eberhard Karls University Tübingen, Tübingen, Germany

ARTICLE INFO

Keywords:
Organ-on-Chip
Microphysiological systems
Optical sensors
Noninvasive readouts
Metabolism
Electrical stimulation

ABSTRACT

Over the last decade, Organ-on-Chip (OoC) emerged as a promising technology for advanced *in vitro* models, recapitulating key physiological cues. OoC approaches tailored for cardiac tissue engineering resulted in a variety of platforms, some of which integrate stimulation or probing capabilities. Due to manual handling processes, however, a large-scale standardized and robust tissue generation, applicable in an industrial setting, is still out of reach. Here, we present a novel cell injection and tissue generation concept relying on spheroids, which can be produced in large quantities and uniform size from induced pluripotent stem cell-derived human cardiomyocytes. Hydrostatic flow transports and accumulates spheroids in dogbone-shaped tissue chambers, which subsequently fuse and form aligned, contracting cardiac muscle fibers. Furthermore, we demonstrate electrical stimulation capabilities by utilizing fluidic media connectors as electrodes and provide the blueprint of a low-cost, open-source, scriptable pulse generator. We report on a novel integration strategy of optical O_2 sensor spots into resin-based microfluidic systems, enabling *in situ* determination of O_2 partial pressures. Finally, a proof-of-concept demonstrating electrical stimulation combined with *in situ* monitoring of metabolic activity in cardiac tissues is provided. The developed system thus opens the door for advanced OoCs integrating biophysical stimulation as well as probing capabilities and serves as a blueprint for the facile and robust generation of high density microtissues in microfluidic modules amenable to scaling-up and automation.

1. Introduction

Microfluidic Organ-on-Chip (OoC) systems have emerged over the last decade as auspicious alternative to conventional cell culture methods, enabling the generation of tissues in precisely controlled environments featuring vasculature-like perfusion. Numerous OoCs culturing single tissues or even combinations of multiple organs have been presented as well as their applicability for mechanistic biomedical research, personalized medicine, and drug testing.

Since cardiotoxicity plays a major role, not only in the drug development process, various Heart-on-Chip (HoC) platforms mimicking the native myocardium (i.e. generating an aligned cardiac muscle fiber) have been developed [1–4]. However, the bare generation of more physiologically relevant model systems is only a first step in investigating and understanding human (patho)physiology. For gaining advanced insights, it is just as important to monitor the effects of precisely controlled external stimuli and to record tissue-specific key parameters [5]. Therefore, one major goal in OoC technology is a direct chip integration of mentioned capabilities.

Due to the unique excitability of cardiac tissue, one of the most important stimuli is electrical stimulation. Pacing can, e.g., be used for advancing tissue maturation or for synchronization of tissue beating, yielding a defined baseline for controlled drug testing [3,6]. Current microphysiological systems integrate pacing capabilities with varying degrees of fabrication complexity, e.g., by utilizing substrate-integrated thin film electrodes, integrating wires into the chip, or fabricating

Abbreviations: OoC, Organ-on-Chip; HoC, Heart-on-Chip; CMs, Cardiomyocytes; hiPSCs, human induced pluripotent stem cells.

* Corresponding author. Fraunhofer Institute for Interfacial Engineering and Biotechnology IGB, Stuttgart, Germany.
E-mail address: peter.loskill@uni-tuebingen.de (P. Loskill).

https://doi.org/10.1016/j.mtbio.2022.100280
Received 16 February 2022; Received in revised form 1 May 2022; Accepted 2 May 2022
Available online 7 May 2022

conductive polydimethylsiloxane (PDMS) pillars [7–9]. In addition to electrical stimulation, mechanical, chemical, or combined stimulations have been presented [10–12].

Similarly, various approaches have been pursued for directly integrating sensing capabilities into HoCs, offering insights into electrophysiology, barrier integrity, or O_2 levels [13–16]. As O_2 plays a key role in regulating cell functions and O_2 consumption can provide crucial insights into cell state and tissue metabolism, the *in situ* determination of O_2 concentration is of particular interest. More broadly, a simple sensor integration is not only of relevance for O_2 monitoring or for cardiac OoCs in general but universally desired for all tissue types. For this purpose, luminescent optical sensor spots are an elegant approach as they can be integrated into microphysiological systems without the need of a wired chip connection, offering on-demand readout opportunities [17–19].

For an accurate recapitulation of native cardiac tissue, high cell densities leading to an abundance of cell-to-cell contacts within cultured tissue construct are crucial. Due to the post-mitotic nature of cardiomyocytes (CMs), the required cell density has to be already achieved during the initial cell injection process. Nevertheless, many systems currently rely on the injection of cell-laden hydrogels, yielding low cell densities. On the other hand, flow-based injection of cell suspensions usually deploys micron-sized retaining features for accumulating cells in defined geometries which are, however, prone to clogging during the loading process, yielding uncontrolled loading pressures, ceasing of flow, and low densities.

As a promising alternative, we recently presented centrifugation-based cell injection techniques [20,21]. Generally, however, the injection of single cell suspensions strongly relies on a well singularized suspension and is prone to inhomogeneities, lacking robustness due to naturally occurring polydispersity. Contrary, spheroids of CMs can be generated with precisely controlled dimensions and have been shown to be able to fuse to arbitrary tissue shapes or be guided inside microfluidic environments [22–24].

Here, we present a novel OoC loading and tissue generation concept based on the introduction of preformed spheroids of controlled size and defined cellular composition into dogbone-shaped tissue chambers via a facile and robust hydrostatic loading. The individual spheroids, formed from human induced pluripotent stem cell (hiPSC) derived CMs as well as fibroblasts subsequently merge to an aligned beating cardiac μ-tissue inside the microfluidic system. Moreover, we demonstrate the integration of both electrical pacing as well as O_2 readout capabilities into the HoC. By using existing fluidic media connectors as electrodes, we confirm reliable tissue excitation with minimal changes in the experimental setup, without the need for advanced fabrication techniques. We report on a newly developed, remotely controllable, "do-it-yourself (DIY)" pacemaker, a valuable alternative to specialized cost-intensive experimental hardware. Furthermore, we introduce a novel strategy for integrating luminescent optical sensor spots into microphysiological platforms by assembling the chip directly from photocurable polymer on top of a sensor substrate. By ultimately combining stimulation and probing capabilities, we reveal changes in O_2 consumption of cardiac tissues upon varying electrical stimulation inside the HoC.

2. Materials and methods

2.1. Chip fabrication

The HoC is composed of a polyethylene-terephthalate (PET) bottom layer with deposited O_2 sensors, a tissue layer molded from UV curable resin (NOA 81, Norland adhesive, USA), a media layer made of PDMS, and a track-etched PET membrane with a pore size of 3 μm (03044, SABEU, Germany), functionalized via plasma-enhanced chemical vapor deposition [25]. The media layer and tissue layer patterning stamp were manufactured by soft lithography and replica molding with PDMS [26]. Briefly, SU-8 based (SU-8 50 & SU-8 100, MicroChem, USA) silicon wafer masters were fabricated according to the manufacturer's protocols (media layer: positive structures, 150 μm high SU8-100 channels; tissue stamp: negative structures, 150 μm high SU-8 100 channels and 30 μm high SU8-50 constrictions). Trichloro (1H,1H,2H, 2H-perfluorooctyl) silane (448931, Sigma-Aldrich, USA) was vapor deposited on both masters for 1 h to facilitate demolding of PDMS. PDMS (Sylgard 184, Dow Corning, USA) was mixed (10:1 base to curing agent mass ratio), degassed and poured onto the wafers. After overnight curing at 60 °C, 3 mm thick PDMS replicates were peeled off the wafer and cropped to chip size. Inlets for media and tissue channels were punched into the media layer with a biopsy puncher (504,529, World Precision Instruments, Germany). Access ports for resin injection were punched with a biopsy puncher (504531, World Precision Instruments, Germany) in all four corners of the injection cavity region of the tissue patterning stamp.

PDMS replicas of the media layer were cleaned with isopropanol (IPA) and residual particles were removed using adhesive tape (56002-00001-01, Tixo, Austria). PET-membranes were cut to desired size using a CO_2 laser cutter (VLS2.30, Universal Laser Systems, USA) and rinsed in ethanol. Following O_2 plasma treatment of both parts (15 s, 50 W; Zepto, Diener, Germany), the media layer was aligned with a membrane covering both chambers. The assembly was baked at 60 °C for 2 h and stored until further usage.

The oxygen indicator dye platinum (II)meso-tetra(4-fluorophenyl) tetrabenzoporphyrin (Pt-TPTBPF) was synthesized as previously described [27]. A stock solution of 10% polystyrene (260 kDa) in Toluene was prepared. 1 mg oxygen indicator dye was added to 1 g stock solution, yielding a concentration of 1% dye in polymer after solvent evaporation. The solution was homogenized by vigorous stirring for 10 min.

PET films (Melinex® 506, DuPont Teijin Films, USA) with a thickness of 125 μm were used as bottom layers. The sensor solution was applied using a microdispenser (MDS3200+, VERMES Microdispensing GmbH, Germany) equipped with a 70 μm nozzle and tungsten tappet with a tip diameter of 0.7 mm. The microdispenser was mounted on a custom-made CNC platform for precise positioning of sensor spots. Detailed printing parameters are listed in Table T1.

The PET films were rinsed with IPA, blow dried, treated with O_2 plasma (60 s, 50 W; Zepto, Diener, Germany) and covered with a solution of 1% (3-Aminopropyl)triethoxysilan (APTES, A3648, Sigma-Aldrich, USA) dissolved in deionized (DI) water. After 10 min, the films were rinsed with DI water and blow dried. The tissue stamps were cleaned with IPA and adhesive tape, and aligned onto the PET films, ensuring full contact of stamp structures with the films while avoiding collapsing of the glue injection cavity. NOA 81 was inserted into 10 ml syringes (BD Plastipak, BD, USA) with attached dispensing tip (21 GA; KDS212P, Weller, USA) and both resin injection ports were filled to the top. Resin immediately started to fill the microcavities. For complete molding, injection ports were filled again after a stopping of filling was observed. After 20 min, the microcavities were completely filled and the assemblies exposed to UV light at 188 mJ/cm^2 ($\lambda = 365$ nm; LED UV mini-Oven, Novachem, Ireland). The stamps were carefully removed, cleaned with adhesive tape and stored for repeated use. The previously prepared media layer-membrane assemblies were cleaned with IPA and adhesive tape (avoiding the area covered by the membrane). Following plasma treatment (60 s, 50 W; Zepto, Diener, Germany), the surface of the assemblies was covered with a 1% APTES solution in DI water for 10 min. The assemblies were then rinsed in DI water, blow dried and aligned onto the resin-based tissue layers. Slight pressure was applied to remove trapped air bubbles and the entire assembly was cured with UV light at 21 J/cm^2 ($\lambda = 365$ nm; LED UV mini-Oven, Novachem, Ireland). The finalized chip was baked for 12 h at 60 °C to improve adhesion. Channels were rinsed with ethanol to remove any remaining, potentially cytotoxic, glue components and left to dry.

2.2. Cell culture

2.2.1. hiPSC culture and CM differentiation

CMs were differentiated from the hiPSC line, Coriell GM25256 (RRID:

CVCL_Y803, Gladstone Institute for Cardiovascular Disease, San Francisco, USA). After thawing, hiPSCs were plated on growth factor-reduced Matrigel (354277, Corning, USA)-coated 6-well plates at a density of 25,000 cells/cm^2 and cultured in TeSR-E8 (05990, STEMCELL Technologies, Canada) medium, supplemented with 10 μM ROCK inhibitor Y-27632 (RI; 05990, STEMCELL Technologies, Canada) for the first 24 h after thawing or passaging. HiPSCs were passaged with Accumax (SCR006, Sigma-Aldrich, USA) at least once before initiation of differentiation.

Differentiation was achieved using an optimized protocol for the small-molecule manipulation of Wnt signaling adapted from Lian et al. [28] Upon reaching ≥90% confluence, (day 0) media was exchanged to RPMI 1640 medium (RPMI; 1185063, Gibco, USA) supplemented with B27 supplement without insulin (B27–I; A1895601, Gibco, USA) and 10 μM of the Wnt agonist CHIR99021 (CHIR; S2924, Selleckchem, USA). Exactly after 24 h, medium was changed to RPMI + B27–I. Two days later (day 3), the medium was changed to RPMI + B27–I with 5 μM Wnt inhibitor IWP-4 (SML1114, Sigma-Aldrich, USA) and incubated for 48 h. On day 5, medium was changed to RPMI + B27–I and on day 7 to RPMI 1640 supplemented with B27 complete supplement (B27C; 17504044, Gibco, USA), which was used thereafter for CM culture, and exchanged every second day. At around day 9–12, cells showed spontaneous beating. On day 15, cells were dissociated by incubation with 280 U/ml Collagenase (LS004174, Worthington, USA) and 40 U/ml DNase (LS006331, Worthington, USA) in RPMI + B27C for 1.5 h. Detached monolayers were collected in a 50 ml conical centrifuge tube containing 20 ml of PBS-, centrifuged at 200×*g* for 3 min and resuspended in Accumax solution followed by 25 min of incubation at 37 °C. After singularization, cells were washed and resuspended in RPMI + B27C with 10 μM of RI. At this point, CM purity was checked by flow cytometry (Guava® easyCyte 8HT, Merck Millipore, USA) for the cardiac marker Cardiac troponin T conjugated to APC (cTnT; 1:50; REA400; 130-120-543, Miltenyi Biotec, Germany). Cells were frozen in RPMI + B27C with 10 μM of RI + 10% FCS +10% DMSO. Only hiPSC-derived CMs with purity ≥80% were used for further experiments.

Before loading, CMs were thawed in RPMI + B27C with 10 μM of RI and plated at a cell density of 2 Mio cells/well in a 6-well plate coated with Matrigel. After 24 h, media was exchanged to RPMI + B27C and after 3 days of culture, cells were used for experiments.

2.2.2. Primary human dermal fibroblasts

Primary human dermal fibroblasts (phDF) were isolated from juvenile foreskin and expanded in culture. 1 million cells were plated in a T175 flask in DMEM (P04-04515, Pan-Biotech, Germany) supplemented with 10% FCS and 1% P/S (DMEM complete). Media was changed every 3 days. After 7 days, the cells were confluent and were either passaged or cryopreserved in DMEM media +10% FCS +10% DMSO. Cells were passaged at least once before any experiment and only used for experiments up to passage 9. PhDF were analyzed by flow cytometry using CD90 antibody conjugated to APC-Vio770 (CD90; 1:50; REA897; 130-114-905, Miltenyi Biotec, Germany).

2.2.3. Spheroid formation

Spheroids were formed following a previously established approach [29]: Briefly, wells of a 6-well microwell culture plate (AggreWell™400, STEMCELL Technologies, USA) were replicated out of Hydrosil (101301, SILADENT, Germany) [30]. Both silicone components were mixed (1:1 wt), 2.5 g was added into each well and the well plate was centrifuged at 55×*g* for 60 s. After curing the silicone for 1 h at 60 °C, well replicas were carefully removed, and circular segments punched out (d = 20 mm). Circular segments were glued with an epoxy adhesive (UHU PLUS sofortfest, UHU, Germany) to a PMMA holder such that the structured side represented the bottom surface of a well (d = 15.5 mm, h = 2 mm) which could be remolded with agarose, fitting into a well of a 24-well plate.

This reusable master mold was sterilized with 70% ethanol before every experiment. 650 μl of 3% agarose solution in DMEM, liquified by preheating in a microwave, was deposited onto the master mold and solidified within 10 min. Once solid, agarose molds were inserted into wells of a 24-well plate with the structured side pointing upwards. 1 ml/well of PBS- was then added to each well and the well plate centrifuged at 1300×*g* for 3 min to remove any air bubbles trapped at the bottom of the inverted pyramid microstructure.

CMs and phDFs were dissociated by incubation with 0.05% Trypsin/Versene for 10 min at RT. Wells were flushed with respective media and cells transferred into a 15 ml conical centrifuge tube and centrifuged for 3 min at 200×*g*. CMs were resuspended in RPMI + B27C containing 10 μM of RI, phDF in DMEM complete. Cells were mixed at a ratio of 3:1 (CMs: phDFs). A total of 0.5 Mio cells were added to each well and centrifuged at 300×*g* for 3 min with a deceleration ramp setting of 3. Cells were incubated (37 °C, 5% CO_2) for 24 h. The next day, around 1200 spheroids/well were formed and could be used for chip loading.

2.2.4. Loading protocol

Chips were treated with O_2 plasma (60 s, 50 W; Zepto, Diener, Germany) for sterilization and hydrophilization and subsequently either filled with a fibronectin solution (20 μg/ml in PBS-; F1141, Sigma-Aldrich, USA) for coating or with pre-warmed media. For coating, chips were incubated for 2 h (37 °C). Pipet tips with 100 μl media were inserted into all tissue and media access ports and remaining air bubbles removed by manual flushing. Spheroids were removed from the well, collected in a 50 ml conical centrifuge tube and sedimented by gravity. Supernatant was aspirated and the spheroids were resuspended in 250 μl/well of RPMI + B27C. 100 μl media were added to the tissue inlet tip followed by 30 μl of spheroid suspension. The difference in liquid column height led to a hydrostatic flow dragging spheroids within several minutes into the cultivation chamber, where they accumulated due to the constricting channel height. The loading process was monitored with a microscope, such that additional spheroids could be added to the inlet tip if the initial number of spheroids was not sufficient.

2.2.5. Chip culture

Following satisfactory loading, media inlet and outlet tips were topped with additional 150 μl of media and the chips were placed in a CO_2-controlled incubator (5% CO_2, 37 °C, 95% relative humidity) overnight. The next day, pipet tips were removed from the tissue channel and corresponding ports sealed with stainless steel plugs. The media channel was subsequently perfused with media at a constant flow rate of 50 μl/h using an external syringe pump (LA-190, Landgraf HLL, Germany). For pacing and O_2 monitoring experiments, chips were removed with corresponding syringes from the incubator, placed into a cell culture hood with incubation conditions (5% CO_2, 37 °C, 72% relative humidity; Incubator FlowBox™, ALS, Germany) and reattached to the syringe pump.

2.3. Immunofluorescence staining

Tissues were fixed inside the chips at room temperature for 15 min by inserting a 4% solution of Roti®Histofix (P087, Carl Roth, Germany), and then permeabilized for 15 min with 0.1% Triton X-100 (28314, Thermo Fisher Scientific, USA). The media layer was then removed, facilitated by a weaker bonding of the membrane-covered region between tissue and media layers. After blocking for 1 h by adding a drop of 3% bovine serum albumin (A9418, Sigma-Aldrich, USA) on the exposed tissues, the tissues were incubated with staining buffer overnight at 4 °C. The staining buffer was composed of APC conjungated cTnT antibody (final dilution: 1:50), DAPI (1 mg/mL, final dilution: 1:250; D9542 Sigma-Aldrich, USA), 0.1% Saponin (84510-100G, Sigma-Aldrich, USA), and 0.1% bovine serum albumin (A9418, Sigma-Aldrich, USA), diluted in PBS^-. Between each step, tissues were flushed with PBS^-. For imaging, the chips were flipped onto #1.5 coverslips and imaged with magnifications of up to 63× using a laser scanning microscope (LSM 710; Zeiss, Germany).

2.4. Characterization of beating motion

Contraction and relaxation motion was analyzed in recorded videos of beating cardiac tissues with OpenHeartWare v1.3 (https://github.com/loslab/ohw) using the optical flow algorithm with a block width of 16 pixels, delay of 2 frames and maximum shift of 7 px. For 1D representations of beating kinetics, mean absolute motion was calculated from obtained vector field. Peak positions were automatically detected, and corresponding beating frequencies determined.

2.5. Simulation of electrical field distribution

Electrical field strength within the paced chip was simulated using finite elements (COMSOL Multiphysics® v5.6, COMSOL AB, Sweden) in a stationary study with the electric currents physics interface. Electrodes were modeled as cylinders in media inlet and outlet with a potential difference of U = 10 V between the surfaces of both electrodes. PDMS was treated as insulator and a conductivity of $\sigma = 1.5$ S/m and relative permittivity of $\varepsilon_r = 80.1$ was assigned to the media domain, adapting previously published material parameters [8]. The absolute field strength was calculated from individual spatial components and plotted in the vertical midplane of the media channel (z = 305 μm) and the tissue chamber (z = 90 μm).

2.6. Pacing of tissues

Tissues were field-paced using the custom-built Arduino-based electrical stimulator "Easypace". The stimulator was able to deliver biphasic pulses ($U = -U_0$ for $t = t_w$, followed by $U = +U_0$ for $t = t_w$, repeated after $t = 1/f$) in adjustable 0.1 Hz frequency steps, 1 ms pulse width steps at an amplitude of up to $U_0 = 12.5$ V and allowed a scripted control of pacing parameters. We provide extensive build-instructions for this cost-efficient (<100 €) open-source tool (https://github.com/loslab/easypace/). If not stated otherwise, a pulse width of $t_w = 50$ ms and amplitude of $U_0 = 10$ V was used; these parameters were determined as most robust for inducing pacing in the HoC.

2.7. Optical analysis of O_2

Chips were fixed with magnets on a custom-built sensor platform consisting of a PMMA plate containing cutouts with geometrically matching sensor positions of four adjoining chips. Optical fibers could be press fitted into the cutouts, enabling a flexible configuration of the measurement setup, e.g., measuring signals of both sensor spots of two chips, or measuring signals of one sensor spot per chip of four chips in total. Sensors were read out using a 4-channel phasefluorimeter (FireSting pro, Pyroscience, Germany) with connected optical fibers (d = 1 mm, l = 1 m). The phasefluorimeter was set to an illumination intensity of 100% and detection amplification of 400 x. Chips were manually aligned for an optimal positioning of the sensor spot above the fiber, yielding signal intensities above 100 mV for every measurement. All measurements were carried out with the same phase shift calibration, previously obtained from a phase shift measurement of the bare sensor substrate at 37 °C, covered with well-aerated water ($pO_2 = 100\%$, $\Delta\varphi = 20.4°$) or a 10% Na_2SO_3 solution ($pO_2 = 0\%$, $\Delta\varphi = 53.8°$).

3. Results

3.1. Concept of the SpheroFlow HoC system

3.1.1. Tissue generation

The underlying tissue generation concept relies on an initial formation of multicellular 3D cardiac μ-tissues (Fig. 1 A). Spheroid formation is a widely established technique yielding 3D tissues without the use of hydrogel. Spheroids can be generated with precisely controlled cellular tissue composition by mixing defined ratios of different cell types, such as CMs and fibroblasts (FBs). While achieving physiological densities and cell-to-cell contacts, they cannot control structural organization and cell alignment, recapitulating tissue structures only partially. The Spheroflow HoC concept is based on injection of pre-formed spheroids into tissue chambers featuring a dogbone-shaped geometry leading to a subsequent fusion of the individual spheroids to uniaxially aligned cardiac muscle fibers.

3.1.2. Loading mechanism

The design of the tissue layer enables the injection of the spheroids simply by hydrostatic pressure driven flow. The layer features structures of two different heights, namely a channel of 180 μm ending in a dogbone-shaped tissue chamber and a channel with a height of 30 μm. Spheroids are loaded into the tissue chamber by adding the spheroid suspension into a pipet tip in the tissue channel inlet. The difference in liquid column height, with respect to the tissue outlet, induces a hydrostatic flow, dragging spheroids into the channel (Fig. 1B i). As the channel constricts at the end of the tissue chamber to the narrow channel height, spheroids are not flushed to the outlet port and accumulate inside the tissue chamber (Fig. 1 B ii). Clogging of the channel is avoided by a narrow side channel into which spheroids cannot penetrate, such that a constant flow is maintained during filling. By exploiting a defined spheroid size (d = 150 μm), the chamber is thus completely filled. Introduced spheroids subsequently merge, forming an aligned tissue, tailored by the channel geometry (Fig. 1 B iii). After loading, the tissue channel ports are closed using metal plugs. The chip is connected to a syringe pump and perfused at defined, constant flow rate. Within the chip the convective media flow is confined to the media channels. The porous membrane separating tissue chambers and media channels, however, allows for diffusion of dissolved O_2, nutrients or other factors from the perfusing media to the tissue and of metabolites and secreted factors from the tissue into the media channel (Fig. 1 C). The perfused media can be collected as effluent after exiting the outlet ports.

3.1.3. Electrical stimulation & sensor integration

In addition to a simplified cardiac μ-tissue generation, the Spheroflow HoC directly integrates probing and analysis capabilities. It provides electrical stimulation of cultured tissues and a readout of O_2 levels via luminescent sensor spots integrated into the bottom of the tissue chamber. The integration of O_2 sensor spots in the knob regions directly below the tissues allows for real-time measurements of O_2 concentrations at tissue level (Fig. 1 B iii). Both features can be combined to study the effects of pacing on O_2 consumption (Fig. 1 D).

No specialized fabrication procedure is needed for adding pacing capabilities, as stimulation is carried out by harnessing fluidic media connectors as electrodes. Instead of flushing a sensor layer into the assembled chip or depositing individual spots into preassembled chip components, the tissue layer is directly fabricated on a sensor substrate via micromolding of the thiolene based resin NOA 81. Patterning of NOA 81 with PDMS molds was introduced a decade ago as a simple and fast method for the generation of through-hole microfluidic stencils and its suitability for microphysiological systems has been demonstrated [31–33]. By combining a tissue layer made out of O_2 impermeable resin with an O_2 permeable media layer made out of PDMS, we generate a precisely controlled probing environment [34]. O_2 is introduced into the tissue chamber only via defined diffusion through the membrane, such that the sensor readout is not influenced by O_2 diffusing from the bottom or side walls.

The developed fabrication concept involves an initial deposition of O_2 sensor spots at defined positions via a CNC-controlled microdispenser onto the bottom layers, adhesive treated PET films (Fig. 2 A i).

To ensure robust bonding between the UV resin tissue layers and the

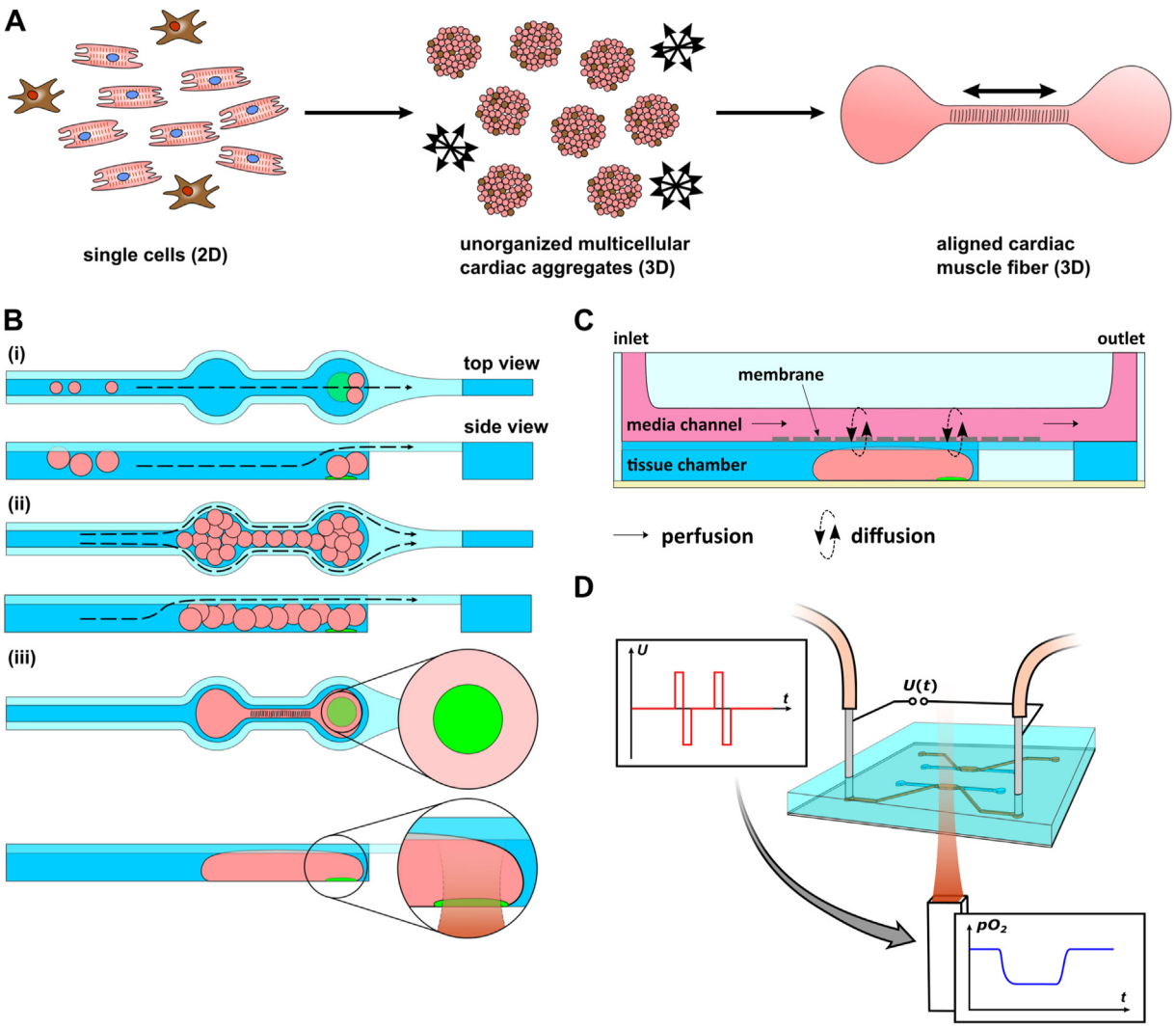

Fig. 1. Concept of the Spheroflow HoC: A) Process for generating aligned cardiac fibers: Initial compaction of single cells of precisely defined mixture to 3D spheroids. Spheroids further merge to an aligned tissue fiber, guided by the chamber geometry. Double headed arrows indicate alignment direction. B) Chip loading mechanism: (i) Spheroids are introduced by hydrostatically driven flow into the dogbone-shaped tissue compartment and confined by the channel constriction. (ii) With gradual filling, the loading flow is maintained by the flanking constriction channel. (iii) Individual spheroids merge to a single aligned cardiac tissue. Embedded O_2 sensor in the knob region enables *in situ* readout of O_2 levels. C) Side view of the chip depicting the nutrient supply: A syringe pump generates a defined media flow in the media channels. The porous membrane protects the cultured tissue from excessive shear forces while allowing diffusive transport of nutrients and waste products. D) Investigation of metabolic activity in perfused tissues. Presented platform enables electrical tissue stimulation coupled to optical readout of O_2 levels.

bottom layers, they are functionalized with APTES (Fig. 2 A ii). A stamp made out of PDMS, replicating the desired microstructure of the tissue layer, incorporating regions of various channel heights for channel and constriction, is placed onto the substrate. The stamp is precisely aligned, matching the second knob (in flow direction of the dogbone-shaped loading chamber) to the sensor spot (Fig. 2 A iii). As the spot can be considered flat compared to the channel structures ($h < 5$ µm), the elastic stamp covers the spot completely, circumventing coverage with resin in the following steps. Resin is injected into the stamp injection port and completely fills the void, corresponding to prospective channel walls, within 30 min (Fig. 2 A iv + v). The whole assembly is exposed to UV light, solidifying the bulk of the injected resin (Fig. 2 A vi). However, resin in contact with PDMS remains uncured, as the O_2 permeability of PDMS leads to localized availability of O_2, preventing full curing in the contact region. After removal of the stamp, tissue channel geometries are thus replicated with a sticky surface of uncured resin, integrating the sensor spot into the channel without covering the sensor in resin (Fig. 2 A vii). The media layer featuring channels replicated in PDMS and a bonded PET membrane, is treated with APTES and aligned with the tissue layer (Fig. 2 A viii). APTES treatment enables a thorough curing without cure inhibition and thus subsequent bonding of resin to the PDMS layer [35]. Finally, the assembly is cured with UV light. One major benefit of the developed fabrication procedure is the reusability of the PDMS stamps (tested for >10 molding cycles). The implemented chip design comprises two independent loading channels, separated by a porous membrane from the respective media channels. One O_2 sensor spot is integrated into the rear knob of each tissue chamber (Fig. 2 B). Finalized microphysiological system consists of a thin bottom layer, integrated sensors, and allows for fluidic connections via the PDMS top layer (Fig. 2 C).

3.2. Tissue characterization

Mixtures of hiPSC-derived CMs and phDFs (3:1 cell number ratio) were centrifuged into inverted microwells and reliably aggregated within 24 h to spherical aggregates of homogeneous size ($d \approx 150$ µm) (Fig. 3A). For a defined aggregate composition, CM purity was assessed after each differentiation and only batches with CM purity ≥80% were used.

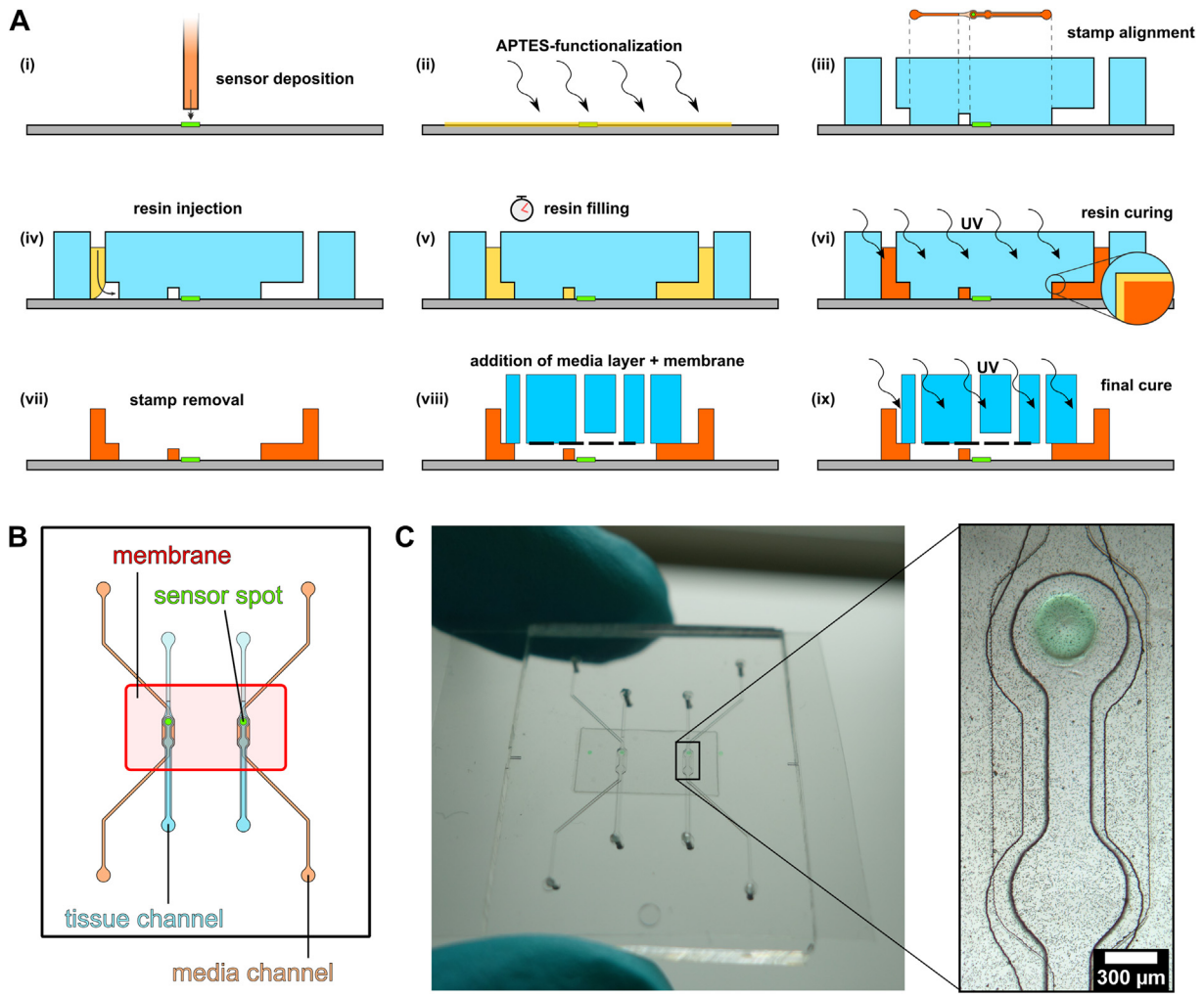

Fig. 2. Microfluidic chip fabrication: A) Microfabrication steps (i-ix): Deposition of O_2 sensor onto bottom layer (i) and subsequent surface functionalization (ii). Placement of PDMS stamp on bottom layer precisely aligning the dogbone-knob onto the sensor spot (iii). Injection (iv), capillary filling (v) and curing (vi) of resin. Resin in contact with PDMS does not solidify due to locally available O_2 and remains sticky (inset). Removal of PDMS stamp exposes open tissue channels with an uncured resin layer (vii). Addition of APTES-treated media layer with bonded membrane (viii) and another UV curing (ix) finalizes the chip. B) Design of Spheroflow HoC: Each chip comprises two individual systems consisting of a loading and media channel, separated by a porous membrane. O_2 sensor spots are integrated into the knob region of the tissue chamber. C) Assembled chip with integrated sensors. Magnified view depicts a micrograph of a dogbone-shaped tissue chamber with integrated O_2 sensor spot.

Similarly, phDFs were characterized during expansion by flow cytometry using the fibroblast marker CD90 (Fig. 3B). Spheroids could be reliably introduced into the HoC, merging within 24 h and forming a compacted, aligned tissue (Fig. 3C, SV1 + SV2). The same loading efficiency and tissue compaction could also be achieved in chips fabricated with a cover slip as bottom layer or chips featuring tissue layers out of PDMS or hot embossed PET-G.

Immunofluorescence staining revealed an alignment of cTnT fibers along the main axis of the dogbone shape (Fig. 3D, S1). Stacked layers of nuclei could be identified along the z-direction, verifying the generation of a 3D tissue. Both highlight that the reorganization of the cells from individual spheroids led to the formation of a single aligned cardiac fiber out of individual µ-tissues.

Three days after chip injection, the tissues typically displayed spontaneous beating. Videos of tissue motion were recorded by video microscopy and analyzed with OpenHeartWare. The spatial distribution of tissue motion indicated a collective ordered motion, confirming again the fusing of individual spheroids to a single unit (Fig. 3E). By averaging the motion of the extracted motion vector field, detailed beating kinetics could be investigated, allowing, e.g., the determination of beating frequency (Fig. 3F, SV3). Peaks of distinct amplitudes attributed to tissue contraction and relaxation are clearly distinguishable.

3.3. *Electrical stimulation of tissues*

Easypace, an Arduino-based pulse generator, was developed to provide a cheap "DIY" platform for electrically stimulating engineered cardiac tissues. It consists of an Arduino-controlled Digital to Analog Converter (DAC) that can create two individual output waveforms, which are subsequently transformed to four independent biphasic pulses by a downstream Operational Amplifier (Fig. 4 A). The pulse generator can be either controlled manually or remotely via Serial commands (Fig. 4 B). Fluidic media connectors out of stainless steel (21 GA; KDS212P, Weller, USA) were harnessed as pacing electrodes and connected via alligator clips to the pulse generator (Fig. 4 C). The theoretical electrical field distribution inside the chip geometry was analyzed using finite elements for a voltage of $U_0 = +10$ V, applied between media inlet and outlet connector. An initial study explicitly modeling individual membrane

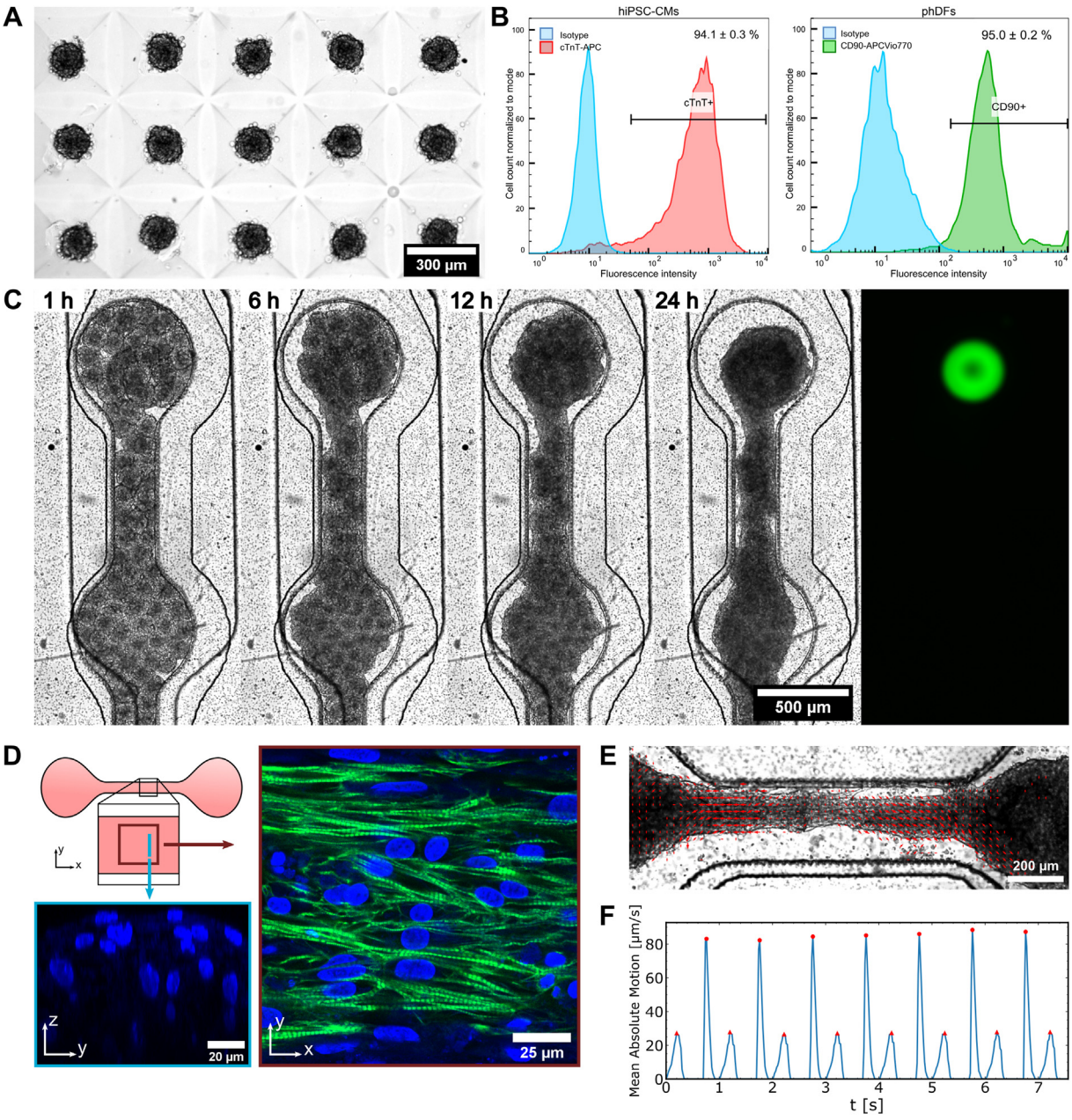

Fig. 3. Formation of cardiac µ-tissues: A) Generation of uniformly sized spheroids in µ-Wells. B) Flow cytometry analysis of CM and FB cell populations prior to spheroid formation. C) Fusing of individual cardiac spheroids to an aligned tissue over the timespan of 24 h after loading. The underlying integrated O_2 sensor spot is visualized via widefield fluorescence microscopy (green, Cy5 filterset). D) Characterization of the structure of the generated cardiac muscle fiber in fibronectin-coated HoC by immunostaining of cTnT (green) and DAPI (blue). The shaft region is characterized by aligned fibers (xy slice). The perpendicular z-stack view reveals stacked nuclei, indicating the generation of a multilayered 3D tissue (yz slice). E) Characterization of beating motion of a fiber. Motion vectors at tissue contraction reveal a collective displacement. F) Optically determined beating kinetics display pronounced peaks of contraction (red circles) and relaxation (red triangles), amenable for beating frequency extraction.

pores revealed negligible influence of the introduced membrane on electrical field distribution, such that the membrane was omitted, accelerating and simplifying simulations. In the horizontal midplane, the simulation predicts a field of $|E| = 0.8$ V/cm that is uniform throughout the tissue chamber shaft region, which is desired for the stimulation of 3D microtissues (Fig. 4 D).

Tissues cultured in Spheroflow chips were field stimulated on day 5 after injection. Distinct pacing frequencies ranging from 0.3 to 2.0 Hz were applied for 10 s per individual frequency and stepwise increased by 0.1 Hz. Videos of beating tissues were recorded simultaneously. By matching timestamps of each pacing frequency interval with recorded video, beating kinetics were investigated for each pacing frequency. (Fig. 4 E, inset). Comparing determined beating frequency with applied pacing frequency, a linear relation up to a maximum pacing frequency is observed (Fig. 4 E). Exceeding this frequency, tissues could not follow the external pacing rate anymore. They skipped every second pulse, yielding a beating frequency half of applied frequency. All investigated tissues could be paced up to 1.5 Hz; individual tissues up to the applied maximum pacing rate of 2.0 Hz. Our findings confirm the applicability of the facile pacing approach via fluidic media connectors. Without the integration of additional electrodes, tissues can be paced and the beating rate precisely controlled.

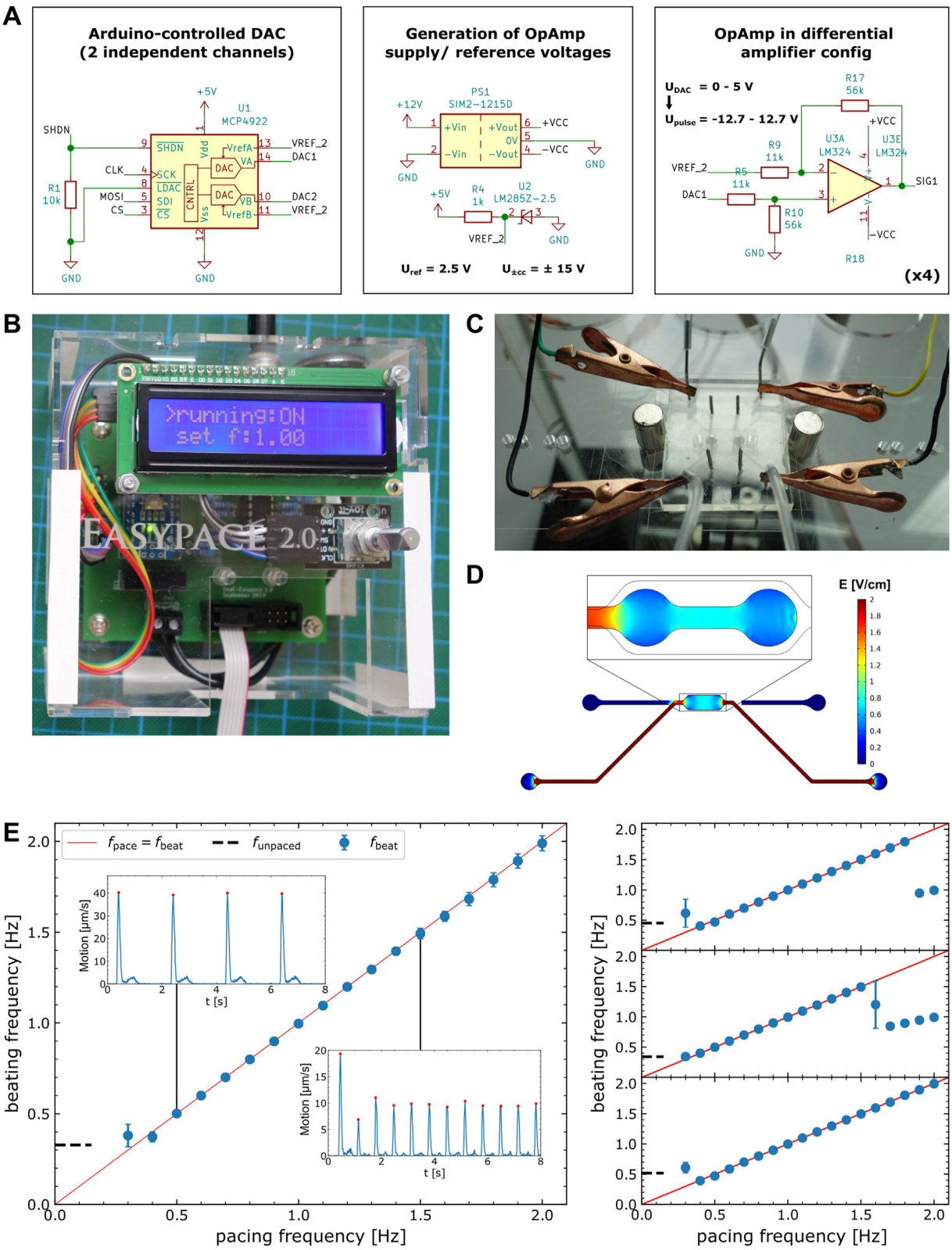

Fig. 4. Electrical stimulation of cardiac tissues: A) Electrical schematic of key components of the pulse generator 'Easypace'. An Arduino-controlled DAC creates two independent output signals that are subsequently converted to biphasic pulses via an Operational Amplifier. B) Picture of the pulse generator 'Easypace' that can be controlled either manually via the rotary encoder or remotely via Serial commands and provides feedback by the integrated LCD display. C) Image of pacing setup. The pulse generator is connected via alligator clips to stainless steel fluidic connectors in the media layer, thus acting as electrodes. D) Simulated electrical field distribution inside media- & tissue-compartments upon application of 10 V between media in- & outlet. E) Beating rate analysis of tissues stimulated electrically at increasing frequencies. Beating frequency extracted from beating kinetics (insets) shown as a function of ramped up pacing frequency for four tissues. Ideal matching of beating and pacing frequency indicated by linear relation (red line).

3.4. Investigation of O_2 levels under varying metabolic activity

To assess the functionality of the integrated O_2 sensing spots, sensor spots in chips with beating cardiac tissues were monitored overnight. Cultured tissues were electrically stimulated by applying a cyclical variation of consecutive biphasic pulses of frequencies 0.7, 1.0, 1.2, and 1.5 Hz. Stimulation was carried out for each frequency for 10 min with a resting phase of 30 min between the application of successive frequency (Fig. 5 A). Each frequency cycle was repeated for three times. In order to exclude any effects of external influences on O_2 levels, pacing cycles were temporally shifted for both paced systems by 20 min with respect to each other. Upon initiation of pacing, a drop in measured O_2 levels can be distinguished, with drop onset clearly coinciding with pacing start (cf. reference line). As in the unpaced reference tissue, constant O_2 levels are detected, this drop can be attributed to a higher O_2 consumption of the tissue that might be caused by increased metabolic activity, triggered by electrical stimulation. Upon termination of pacing, an increase in O_2 levels towards initial partial pressures, monitored in the unpaced state, is observed. Stimulating the other tissue, the identical behavior is detected. Increasing pacing frequencies display increased jumps in O_2 levels. Jump height is determined by the difference between O_2 partial pressure at pacing onset and pacing termination, and evaluated for both tissues as a function of the applied pacing frequency. Jump heights are furthermore normalized to the difference of O_2 partial pressure between the unpaced state and the fully oxygenated state, yielding relative jumps in O_2 concentration (Fig. 5 B). Relative jumps expose for both investigated systems an increase with applied pacing frequency, observable in each pacing cycle.

Signal stability of the sensor chip is investigated by perfusing four empty systems with media in culture conditions (37 °C, 5% CO_2, 50 µl/h). Over the timespan of 12 h, all measured O_2 partial pressures display minimal (<1 hPa/h) shifts, precluding O_2 scavenging of employed resin NOA 81 (Fig. 5 C). Chamber 4 exhibits a spike in O_2 partial pressure, which we attribute to a passing air bubble.

In order to attribute the observed variation in O_2 levels to an increase in tissue O_2 consumption, potential changes in O_2 concentration triggered by electrolysis needed to be excluded: O_2 levels were recorded in an empty chip perfused with media, undergoing electrical stimulation (Fig. 5 D). Two out of four investigated systems were stimulated at the maximum voltage of 12.5 V with initial frequency of 1 Hz, further ramped up to 3 Hz for up to 8 min. No drop in O_2 concentration was detected. Comparing the O_2 partial pressure trend with unpaced chambers, all exhibit a similarly constant trend.

4. Discussion

Many concepts of HoCs have been proposed in recent years. Here, we have presented a novel microphysiological system targeting controlled tissue generation and integrating O_2 sensing and electrical pacing capabilities. The novel tissue generation approach combines the well-established technique of cardiac spheroid formation with OoC technology. Aligned cardiac fibers could be generated out of radially symmetric multicellular cardiac spheroids of defined composition as starting point. Formed tissues are characterized by a fiber alignment at a length scale

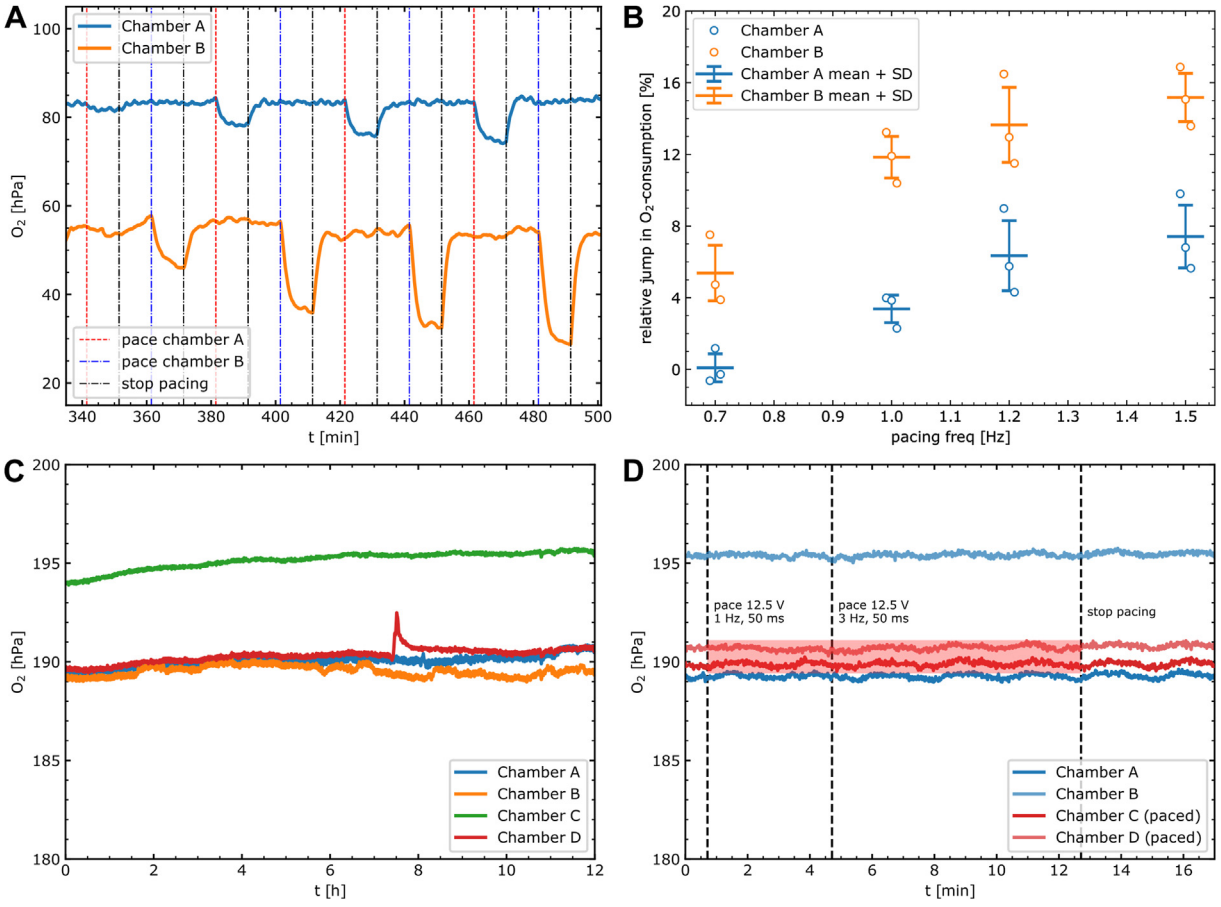

Fig. 5. *In situ* measurements of O_2 levels: A) Recording of O_2 partial pressures of two tissues alternatingly paced (dashed lines) at increasing frequencies of (0.7, 1.0, 1.2, 1.5) Hz. B) Evaluation of frequency dependence of relative jump heights in O_2 consumption for tissues repeatedly probed following timings in (A). C) Stability analysis of O_2 levels in empty systems perfused with media over 12 h. D) Comparison of O_2 partial pressures between paced and unpaced chambers, measured in empty, media-perfused systems. No difference between both conditions is observed, excluding O_2 changes induced by electrolysis.

exceeding individual spheroid size, which indicates a complete rearrangement to one aligned tissue.

The developed approach of preforming spheroids and subsequently merging them on-chip provides a robust loading and standardized μ-tissue generation. Due to the simple loading mechanism, driven by hydrostatic pressure, the presented system offers opportunities for automated tissue generation; feasible even at large-scale, as only simple pipetting steps are necessary which could be carried out by liquid handling robots. Currently, each injection port is connected to only one chamber, a conceivable multiple branching of the injection channel, however, offers potential for parallelization.

Compared to single cells, which can hardly be compacted in a tissue chamber without applying uncontrolled pressures, the utilization of spheroids as building blocks facilitates injection as they can easily be guided by a clogging-free flanking constricted channel to desired positions, providing a robust loading procedure. Compared to the injection of single cells embedded in hydrogel or as a suspension, the use of spheroids provides the advantage of achieving higher cell densities, which better resembles physiological tissue, facilitates cell-to-cell contacts and prevents overgrowth of proliferative cell types such as fibroblasts. Moreover, the pre-formation of spheroids integrating non-CM cell types grants a defined cell composition and a homogenous distribution of embedded cell types throughout the tissue. As reported previously [36], the inclusion of stromal cells within cardiac tissue enhances tissue maturation, robustness and functionality. In order to provide structural support and extracellular matrix (ECM) production capacity to our model, we included human dermal fibroblasts as a proof of concept. For future studies, especially on electrophysiological aspects, the integration of isogenic cardiac fibroblasts is crucial as they offer unique electrical conduction properties [37,38].

We presented a dogbone shaped tissue chamber; the underlying concept, however, is universal, allowing μ-tissue generation in arbitrary formed tissue chambers or even the generation of stratified tissues. As spheroids fill the tissue chamber subsequently, it is also conceivable to consecutively inject spheroids of varying composition, thus creating, e.g., a cardiac fiber featuring fibrotic tissue on one end and healthy tissue on the other end. Furthermore, the concept is not fixed on the utilization of a sensor substrate; we assembled chips of the same design on coverslips for high-resolution imaging and fabricated a pure PDMS based system integrating two micropillars inside the dogbone knobs enabling readouts of contractile force in other studies. The utilized PET films were chosen to provide optimal sensor spot adhesion. We, however, observed hampered imaging qualities for epi-illumination microscopy. Thus, the media layer had to be removed for immunofluorescence imaging. We plan to optimize bottom layer materials in further chip generations, enabling imaging of the chip in the unperturbed state while maintaining sufficient sensor spot adhesion.

We demonstrated a noninvasive integration strategy of electrical pacing capabilities, superseding complex integration of electrodes into the chip for simple pacing purposes, and could verify precise control of beating rate with the chosen approach. Pacing was only investigated for short time periods (up to 10 min); long-term pacing with applied pacing voltage might lead to the creation of toxic byproducts. However, compared to pacing in a static system, we are confident that the media flow would remove toxic byproducts, such that pacing can be also carried out for longer time periods, e.g. for inducing maturation.

We are aware that the predicted field strengths of 0.8 V/cm lie below field strengths often used in literature of 5 V/cm [39]. Utilized parameters, however, still induced robust pacing, which is most probably balanced by an increased pulse width of 50 ms compared to commonly used 5 ms. If higher fields strengths are desired, utilizing tissue channel sealing plugs as electrodes is also feasible, allowing in addition a flexible choice of electrode material.

Within our studies we developed the low-cost pulse generator *Easypace*, which we think is a valuable Open-Source Hardware tool for the scientific community with its easy fabrication and scriptable pacing capabilities. Provided automation capabilities are of special interest for running overnight experiments involving various pacing parameters or frequency sweeps.

Standardization and upscaling of OoC platforms is essential for any application in an industrial setting. The developed novel sensor integration concept is distinguished by its approach of directly fabricating the chip on top of the sensor substrate. Hence, it is not necessary to ship pre-assembled chip components to external facilities for sensor deposition. Standardized sensor substrates, offering a geometrical arrangement of sensor spots on a predefined regular grid, which are not tailored to any specific chip design, could be produced in large quantities in the future and lead to a broader adaption of the integration of sensors into OoC platforms due to wide availability, furthermore guiding chip design.

By integrating the O_2 sensor spots into the bottom of the tissue chambers, the sensors are in direct contact with the tissues, granting *in situ* readouts and minimizing aberrations from spatial oxygen gradients. As the employed UV resin is gas-impermeable and does not exhibit O_2 scavenging properties, a defined configuration with O_2 influx only via the membrane is generated. We did not observe sensor degradation in our one week experiments, in line with reports about high photo-stability of comparable sensors [40]. Comparing signals of various chambers perfused under identical conditions, we noticed slight differences in measured O_2 partial pressures (up to 5 hPa). We attribute these deviations to variations in the manual fabrication process. Slight variations in stamp alignment can lead to partial coverage of the sensor layer with resin. As the covered part is not aerated, this might lead to a biased signal. The same calibration was used for all sensor spots, not accounting for individual variations. We suggest an individual calibration of each sensor in further studies quantifying O_2 consumption rates.

Ultimately, we provided a biological proof-of-concept of combined stimulation and probing inside a HoC, assessing metabolic tissue activity under the influence of external pacing. Integrated O_2 sensors granting fast *in situ* read outs offer huge potential to assess changes in metabolism triggered by other biochemical or mechanical stimuli. Particularly, we see huge potential for an integrated analysis of oxygen consumption rates in cultured μ-tissues, similarly to the Seahorse assay, the gold standard for metabolic measurements. In addition to O_2 sensing, the developed platform can be used to study Ca^{2+} propagation kinetics along the uniaxial cardiac fiber (cf. supplementary information + S2). We determined mean Ca^{2+} propagation velocities within a fiber cultured in the chip to $v_{sig} = 55$ mm/s, coinciding in magnitude with velocities measured in similar systems of 46 mm/s and 95 mm/s [41,42].

All in all, the developed system can be considered a versatile platform opening the door for addressing key biological questions, e.g., investigating maturation via pacing or the effect of administered drugs on O_2 consumption of physiological μ-tissues.

Credit author statement

Oliver Schneider: Conceptualization, Methodology, Investigation, Software, Data curation, Visualization, Writing – original draft; **Alessia Moruzzi**: Methodology, Investigation, Writing – original draft, Writing-Reviewing and Editing. **Stefanie Fuchs**: Conceptualization, Methodology, Writing – original draft; **Alina Grobel**: Investigation; and **Henrike S. Schulze**: Investigation; **Torsten Mayr**: Funding acquisition, Supervision; **Peter Loskill**: Conceptualization, Writing – review & editing, Funding acquisition, Supervision.

Data availability

All experimental data within the article are available from the corresponding author upon reasonable request.

Declaration of competing interest

The authors declare the following competing interest(s): T.M. is a

founder, holds equity in PyroScience GmbH in Germany, and is the CEO of the Austrian branch, PyroScience AT GmbH. PyroScience is a developer, producer, and vendor of sensor technology.

Acknowledgments

The authors would like to thank Sarah J. Rockwood, Ana C. Silva and Todd C. McDevitt at Gladstone Institutes for an introduction and training on spheroid formation and culture.

The research was supported in part by the DAAD funded by the Bundesministeriums für Bildung und Forschung (BMBF) (PPP USA 2018, 57387214) as well as the European Union's Horizon 2020 research and innovation program under the Marie Skłodowska-Curie grant agreement no. 812954.

Appendix A. Supplementary data

Supplementary data to this article can be found online at https://doi.org/10.1016/j.mtbio.2022.100280.

References

[1] I.J. Onakpoya, C.J. Heneghan, J.K. Aronson, Post-marketing withdrawal of 462 medicinal products because of adverse drug reactions: a systematic review of the world literature, BMC Med. 14 (2016) 10, https://doi.org/10.1186/s12916-016-0553-2.

[2] A. Marsano, C. Conficconi, M. Lemme, P. Occhetta, E. Gaudiello, E. Votta, G. Cerino, A. Redaelli, M. Rasponi, Beating heart on a chip: a novel microfluidic platform to generate functional 3D cardiac microtissues, Lab Chip 16 (2016) 599–610, https://doi.org/10.1039/C5LC01356A.

[3] S.S. Nunes, J.W. Miklas, J. Liu, R. Aschar-Sobbi, Y. Xiao, B. Zhang, J. Jiang, S. Massé, M. Gagliardi, A. Hsieh, N. Thavandiran, M.A. Laflamme, K. Nanthakumar, G.J. Gross, P.H. Backx, G. Keller, M. Radisic, Biowire: a platform for maturation of human pluripotent stem cell–derived cardiomyocytes, Nat. Methods 10 (2013) 781–787, https://doi.org/10.1038/nmeth.2524.

[4] A. Mathur, P. Loskill, K. Shao, N. Huebsch, S. Hong, S.G. Marcus, N. Marks, M. Mandegar, B.R. Conklin, L.P. Lee, K.E. Healy, Human iPSC-based cardiac microphysiological system for drug screening applications, Sci. Rep. 5 (2015) 8883, https://doi.org/10.1038/srep08883.

[5] Y.S. Zhang, J. Aleman, A. Arneri, S. Bersini, F. Piraino, S.R. Shin, M.R. Dokmeci, A. Khademhosseini, From cardiac tissue engineering to heart-on-a-chip: beating challenges, Biomed, Mater 10 (2015), 034006, https://doi.org/10.1088/1748-6041/10/3/034006.

[6] K. Ronaldson-Bouchard, S.P. Ma, K. Yeager, T. Chen, L. Song, D. Sirabella, K. Morikawa, D. Teles, M. Yazawa, G. Vunjak-Novakovic, Advanced maturation of human cardiac tissue grown from pluripotent stem cells, Nature 556 (2018) 239–243, https://doi.org/10.1038/s41586-018-0016-3.

[7] N. Zhang, F. Stauffer, B.R. Simona, F. Zhang, Z.M. Zhang, N.P. Huang, J. Vörös, Multifunctional 3D electrode platform for real-time in situ monitoring and stimulation of cardiac tissues, Biosens. Bioelectron. 112 (2018) 149–155, https://doi.org/10.1016/j.bios.2018.04.037.

[8] R. Visone, G. Talò, P. Occhetta, D. Cruz-Moreira, S. Lopa, O.A. Pappalardo, A. Redaelli, M. Moretti, M. Rasponi, A microscale biomimetic platform for generation and electro-mechanical stimulation of 3D cardiac microtissues, APL Bioeng 2 (2018), 046102, https://doi.org/10.1063/1.5037968.

[9] J.K. Yip, D. Sarkar, A.P. Petersen, J.N. Gipson, J. Tao, S. Kale, M.L. Rexius-Hall, N. Cho, N.N. Khalil, R. Kapadia, M.L. McCain, Contact photolithography-free integration of patterned and semi-transparent indium tin oxide stimulation electrodes into polydimethylsiloxane-based heart-on-a-chip devices for streamlining physiological recordings, Lab Chip 21 (2021) 674–687, https://doi.org/10.1039/D0LC00948B.

[10] N. Huebsch, B. Charrez, G. Neiman, B. Siemons, S.C. Boggess, S. Wall, V. Charwat, K.H. Jæger, D. Cleres, Å. Telle, F.T. Lee-Montiel, N.C. Jeffreys, N. Deveshwar, A.G. Edwards, J. Serrano, M. Snuderl, A. Stahl, A. Tveito, E.W. Miller, K.E. Healy, Metabolically driven maturation of human-induced-pluripotent-stem-cell-derived cardiac microtissues on microfluidic chips, Nat. Biomed. Eng. 6 (2022) 372–388, https://doi.org/10.1038/s41551-022-00884-4.

[11] W. LaBarge, S. Mattappally, R. Kannappan, V.G. Fast, D. Pretorius, J.L. Berry, J. Zhang, Maturation of three-dimensional, hiPSC-derived cardiomyocyte spheroids utilizing cyclic, uniaxial stretch and electrical stimulation, PLoS One 14 (2019), e0219442, https://doi.org/10.1371/journal.pone.0219442.

[12] S.M. Santoni, T. Winston, P. Hoang, Z. Ma, Microsystems for electromechanical stimulations to engineered cardiac tissues, Microphysiological Syst 2 (2018) 11, https://doi.org/10.21037/mps.2018.11.01, 11.

[13] A. Moya, M. Ortega-Ribera, X. Guimerà, E. Sowade, M. Zea, X. Illa, E. Ramon, R. Villa, J. Gracia-Sancho, G. Gabriel, Online oxygen monitoring using integrated inkjet-printed sensors in a liver-on-a-chip system, Lab Chip 18 (2018) 2023–2035, https://doi.org/10.1039/C8LC00456K.

[14] F. Qian, C. Huang, Y.-D. Lin, A.N. Ivanovskaya, T.J. O'Hara, R.H. Booth, C.J. Creek, H.A. Enright, D.A. Soscia, A.M. Belle, R. Liao, F.C. Lightstone, K.S. Kulp, E.K. Wheeler, Simultaneous electrical recording of cardiac electrophysiology and contraction on chip, Lab Chip 17 (2017) 1732–1739, https://doi.org/10.1039/C7LC00210F.

[15] B.M. Maoz, A. Herland, O.Y.F. Henry, W.D. Leineweber, M. Yadid, J. Doyle, R. Mannix, V.J. Kujala, E.A. FitzGerald, K.K. Parker, D.E. Ingber, Organs-on-Chips with combined multi-electrode array and transepithelial electrical resistance measurement capabilities, Lab Chip 17 (2017) 2294–2302, https://doi.org/10.1039/C7LC00412E.

[16] S. Fuchs, S. Johansson, A.Ø. Tjell, G. Werr, T. Mayr, M. Tenje, In-line analysis of organ-on-chip systems with sensors: integration, fabrication, challenges, and potential, ACS Biomater. Sci. Eng. 7 (2021) 2926–2948, https://doi.org/10.1021/acsbiomaterials.0c01110.

[17] B. Müller, P. Sulzer, M. Walch, H. Zirath, T. Buryška, M. Rothbauer, P. Ertl, T. Mayr, Measurement of respiration and acidification rates of mammalian cells in thermoplastic microfluidic devices, Sensor. Actuator. B Chem. 334 (2021) 129664, https://doi.org/10.1016/j.snb.2021.129664.

[18] H. Zirath, M. Rothbauer, S. Spitz, B. Bachmann, C. Jordan, B. Müller, J. Ehgartner, E. Priglinger, S. Mühleder, H. Redl, W. Holnthoner, M. Harasek, T. Mayr, P. Ertl, Every breath you take: non-invasive real-time oxygen biosensing in two- and three-dimensional microfluidic cell models, Front. Physiol. 9 (2018), https://doi.org/10.3389/fphys.2018.00815.

[19] H. Zirath, S. Spitz, D. Roth, T. Schellhorn, M. Rothbauer, B. Müller, M. Walch, J. Kaur, A. Wörle, Y. Kohl, T. Mayr, P. Ertl, Bridging the academic–industrial gap: application of an oxygen and pH sensor-integrated lab-on-a-chip in nanotoxicology, Lab Chip 21 (2021) 4237–4248, https://doi.org/10.1039/D1LC00528F.

[20] O. Schneider, L. Zeifang, S. Fuchs, C. Sailer, P. Loskill, User-friendly and parallelized generation of human induced pluripotent stem cell-derived microtissues in a centrifugal heart-on-a-chip, Tissue Eng. 25 (2019) 786–798, https://doi.org/10.1089/ten.tea.2019.0002.

[21] S. Schneider, F. Erdemann, O. Schneider, T. Hutschalik, P. Loskill, Organ-on-a-disc: a platform technology for the centrifugal generation and culture of microphysiological 3D cell constructs amenable for automation and parallelization, APL Bioeng 4 (2020), 046101, https://doi.org/10.1063/5.0019766.

[22] D.C. Nguyen, T.A. Hookway, Q. Wu, R. Jha, M.K. Preininger, X. Chen, C.A. Easley, P. Spearman, S.R. Deshpande, K. Maher, M.B. Wagner, T.C. McDevitt, C. Xu, Microscale generation of cardiospheres promotes robust enrichment of cardiomyocytes derived from human pluripotent stem cells, Stem Cell Rep. 3 (2014) 260–268, https://doi.org/10.1016/j.stemcr.2014.06.002.

[23] A.C. Daly, M.D. Davidson, J.A. Burdick, 3D bioprinting of high cell-density heterogeneous tissue models through spheroid fusion within self-healing hydrogels, Nat. Commun. 12 (2021) 753, https://doi.org/10.1038/s41467-021-21029-2.

[24] G. Bergström, J. Christoffersson, K. Schwanke, R. Zweigerdt, C.-F. Mandenius, Stem cell derived in vivo-like human cardiac bodies in a microfluidic device for toxicity testing by beating frequency imaging, Lab Chip 15 (2015) 3242–3249, https://doi.org/10.1039/C5LC00449G.

[25] J. Rogal, C. Binder, E. Kromidas, J. Roosz, C. Probst, S. Schneider, K. Schenke-Layland, P. Loskill, WAT-on-a-chip integrating human mature white adipocytes for mechanistic research and pharmaceutical applications, Sci. Rep. 10 (2020) 6666, https://doi.org/10.1038/s41598-020-63710-4.

[26] Y. Xia, G.M. Whitesides, Soft lithography, Angew. Chem. Int. Ed. 37 (1998) 550–575, https://doi.org/10.1002/(SICI)1521-3773(19980316)37:5<550:AID-ANIE550>3.3.CO;2-7.

[27] S.M. Borisov, G. Nuss, I. Klimant, Red light-excitable oxygen sensing materials based on platinum(II) and palladium(II) benzoporphyrins, Anal. Chem. 80 (2008) 9435–9442, https://doi.org/10.1021/ac801521v.

[28] X. Lian, J. Zhang, S.M. Azarin, K. Zhu, L.B. Hazeltine, X. Bao, C. Hsiao, T.J. Kamp, S.P. Palecek, Directed cardiomyocyte differentiation from human pluripotent stem cells by modulating Wnt/β-catenin signaling under fully defined conditions, Nat. Protoc. 8 (2013) 162–175, https://doi.org/10.1038/nprot.2012.150.

[29] T.A. Hookway, J.C. Butts, E. Lee, H. Tang, T.C. McDevitt, Aggregate formation and suspension culture of human pluripotent stem cells and differentiated progeny, Methods 101 (2016) 11–20, https://doi.org/10.1016/j.ymeth.2015.11.027.

[30] J. Dahlmann, G. Kensah, H. Kempf, D. Skvorc, A. Gawol, D.A. Elliott, G. Dräger, R. Zweigerdt, U. Martin, I. Gruh, The use of agarose microwells for scalable embryoid body formation and cardiac differentiation of human and murine pluripotent stem cells, Biomaterials 34 (2013) 2463–2471, https://doi.org/10.1016/j.biomaterials.2012.12.024.

[31] D. Bartolo, G. Degré, P. Nghe, V. Studer, Microfluidic stickers, Lab Chip 8 (2008) 274–279, https://doi.org/10.1039/B712368J.

[32] R. Li, X. Lv, M. Hasan, J. Xu, Y. Xu, X. Zhang, K. Qin, J. Wang, D. Zhou, Y. Deng, A rapidly fabricated microfluidic chip for cell culture, J. Chromatogr. Sci. 54 (2016) 523–530, https://doi.org/10.1093/chromsci/bmv176.

[33] M. Morel, D. Bartolo, J.-C. Galas, M. Dahan, V. Studer, Microfluidic stickers for cell-and tissue-based assays in microchannels, Lab Chip 9 (2009) 1011–1013, https://doi.org/10.1039/B819090A.

[34] Y. Gao, G. Stybayeva, A. Revzin, Fabrication of composite microfluidic devices for local control of oxygen tension in cell cultures, Lab Chip 19 (2019) 306–315, https://doi.org/10.1039/C8LC00825F.

[35] M. Agostini, G. Greco, M. Cecchini, Polydimethylsiloxane (PDMS) irreversible bonding to untreated plastics and metals for microfluidics applications, Apl. Mater. 7 (2019), 081108, https://doi.org/10.1063/1.5070136.

[36] M.E. Floy, T.D. Mateyka, K.L. Foreman, S.P. Palecek, Human pluripotent stem cell-derived cardiac stromal cells and their applications in regenerative medicine, Stem Cell Res. 45 (2020) 101831, https://doi.org/10.1016/j.scr.2020.101831.

[37] E. Ongstad, P. Kohl, Fibroblast–myocyte coupling in the heart: potential relevance for therapeutic interventions, J. Mol. Cell. Cardiol. 91 (2016) 238–246, https://doi.org/10.1016/j.yjmcc.2016.01.010.

[38] J. Zhang, R. Tao, K.F. Campbell, J.L. Carvalho, E.C. Ruiz, G.C. Kim, E.G. Schmuck, A.N. Raval, A.M. da Rocha, T.J. Herron, J. Jalife, J.A. Thomson, T.J. Kamp, Functional cardiac fibroblasts derived from human pluripotent stem cells via second heart field progenitors, Nat. Commun. 10 (2019) 2238, https://doi.org/10.1038/s41467-019-09831-5.

[39] N. Tandon, A. Marsano, R. Maidhof, L. Wan, H. Park, G. Vunjak-Novakovic, Optimization of electrical stimulation parameters for cardiac tissue engineering, J. Tissue Eng. Regen. Med. 5 (2011) e115–e125, https://doi.org/10.1002/term.377.

[40] J. Ehgartner, P. Sulzer, T. Burger, A. Kasjanow, D. Bouwes, U. Krühne, I. Klimant, T. Mayr, Online analysis of oxygen inside silicon-glass microreactors with integrated optical sensors, Sensor. Actuator. B Chem. 228 (2016) 748–757, https://doi.org/10.1016/j.snb.2016.01.050.

[41] B.W. Ellis, A. Acun, U.I. Can, P. Zorlutuna, Human iPSC-derived myocardium-on-chip with capillary-like flow for personalized medicine, Biomicrofluidics 11 (2017), 024105, https://doi.org/10.1063/1.4978468.

[42] A.P. Petersen, D.M. Lyra-Leite, N.R. Ariyasinghe, N. Cho, C.M. Goodwin, J.Y. Kim, M.L. McCain, Microenvironmental modulation of calcium wave propagation velocity in engineered cardiac tissues, Cell. Mol. Bioeng. 11 (2018) 337–352, https://doi.org/10.1007/s12195-018-0522-2.